





A nutrient control on expanded anoxia and global cooling during the Late Ordovician mass extinction

Zhen Qiu ^{1,2✉}, Caineng Zou ^{1,2✉}, Benjamin J. W. Mills³, Yijun Xiong³, Huifei Tao⁴, Bin Lu¹, Hanlin Liu¹, Wenjiao Xiao ^{5,6} & Simon W. Poulton ^{3✉}

Expanded ocean anoxia and global cooling have been invoked as major causal mechanisms for the Late Ordovician mass extinction, but the factors underpinning the extinction remain unresolved. Here, we document two intervals of particularly intense phosphorus recycling in marine rocks deposited across a bathymetric transect in the Yangtze Shelf Sea. The first occurred during the initial phase of the extinction and, coincident with global cooling, drove the development of ocean euxinia on the shelf. The second re-established shelf euxinia after the peak of glaciation, leading to the second phase of extinction. Integration of these data into a global biogeochemical model indicates that phosphorus recycling would have doubled the long-term burial rate of organic carbon, driving $\sim 4^{\circ}\text{C}$ of global cooling. Thus, through its impact on both the spread of anoxia and global cooling, extensive redox-promoted phosphorus recycling was a critical factor in Earth's first catastrophic loss of animal life.

¹Research Institute of Petroleum Exploration & Development, China National Petroleum Corporation, Beijing, China. ²National Energy Shale Gas Research & Development (Experiment) Center, Beijing, China. ³School of Earth and Environment, University of Leeds, Leeds LS2 9JT, UK. ⁴Lanzhou Center for Oil and Gas Resources, Northwest Institute of Eco-Environment and Resources, Chinese Academy of Sciences, Lanzhou, China. ⁵Xinjiang Research Centre for Mineral Resources, Xinjiang Institute of Ecology and Geography, Chinese Academy of Sciences, Urumqi, China. ⁶Institute of Geology and Geophysics, Chinese Academy of Sciences, Beijing, China. ✉email: qiuzhen316@163.com; zcn@petrochina.com.cn; s.poulton@leeds.ac.uk

An estimated 53% of marine species became extinct during the late Ordovician mass extinction (LOME) ~445 million years ago (Ma)¹. This loss of marine fauna is considered to have occurred in two phases, with the initial, major extinction phase (LOMEI-1) occurring at the Katian/Hirnantian stage boundary, and the second interval (LOMEI-2) occurring in the late Hirnantian². Both rapid global cooling leading to the Hirnantian glaciation, and expanded marine anoxia and/or euxinia (anoxic, sulfidic conditions), have been invoked as causal mechanisms for the LOME^{3–8}.

The precise role of each of these mechanisms in driving the LOME is controversial. In part, this is due to uncertainty in stratigraphic correlations between sections used to evaluate the potential roles of glaciation and ocean anoxia, and even mismatches in the timing of the onset of the LOME^{4,5}. However, geochemical evidence from the same stratigraphic sections in the Yangtze Shelf Sea, South China, suggests that expanded euxinia was likely directly responsible for the two pulses of the LOME, with global cooling playing a secondary role⁴. Nevertheless, while there is abundant evidence for water column anoxia at various stages of the LOME^{3–5,9,10}, an integrated understanding of links between water column deoxygenation and coeval global cooling has remained elusive.

Cooling during the late Ordovician has commonly been considered to be due to drawdown of atmospheric CO₂ through global silicate weathering and organic carbon burial. These processes are thought to have been enhanced through mountain building^{11,12} and by the expansion of early land plants^{13–16}. The late Ordovician also saw periods of intense volcanism¹⁷, which may have supplied large amounts of phosphorus (P) through ash deposition and the weathering of tephra¹⁸. Phosphorus is the ultimate limiting nutrient for marine primary productivity on geological timescales¹⁹ and increased P bioavailability due to enhanced volcanism, weathering and/or land plant expansion during the Hirnantian stage may have stimulated primary productivity and contributed to the drawdown of CO₂¹⁸. This increased P influx would also have increased oxygen demand in the water column²⁰, potentially leading to the development of water column anoxia. However, recent biogeochemical modelling has shown that reproducing the amount of cooling evidenced in the geologic record would require substantially more P than was available from the volcanic source¹⁸, and the P supply from weathering and plant expansion is not well known¹⁴.

Phosphorus bioavailability is also closely linked to redox conditions in the ocean and during early diagenesis^{21–25}. During organic matter (C_{org}) remineralization under anoxic conditions in the water column and during early diagenesis, intense preferential recycling of P commonly occurs^{21,22}. This process is particularly prevalent during the microbial generation of dissolved sulfide (which elevates C_{org}/P_{org} values above the Redfield ratio of 106:1), while the reductive dissolution of Fe (oxyhydr)oxide minerals also releases associated P (P_{Fe}) to solution^{21,26}. Some of the released P may undergo ‘sink-switching’ to authigenic phases, such as carbonate fluorapatite (P_{aut})²⁷ or vivianite (which is extracted as part of the P_{Fe} pool)^{28,29}. However, dependent on the precise redox condition of the water column and underlying sediments, P may also be recycled back to the water column, where it has the potential to promote a positive productivity feedback²⁰. Indeed, it has been speculated that such recycling may have played a critical, but unsubstantiated, role in both global cooling and the development of water column anoxia during the LOME¹⁸.

Here, we utilize a P phase partitioning approach³⁰ to provide an empirical reconstruction of the behavior of the P cycle at two locations across a bathymetric transect in the Yangtze Shelf Sea, South China (Fig. 1; Supplementary Note 1; Supplementary Fig. 1). These locations comprise the proximal Shuanghe inner-

shelf (SH) outcrop section and the distal outer-shelf Wuxi (WX) drill core section (Supplementary Notes 2, 3; Supplementary Figs. 2, 3), which were deposited during the Late Ordovician (Katian Stage) to Early Silurian (Rhudanian stage) (Fig. 1). We then integrate these new data into a biogeochemical model to provide detailed constraints on the role of P recycling in both the development of anoxia and global cooling during Earth’s first catastrophic loss of animal life.

Results

Both sections have organic carbon concentrations (see Methods) that start with low values (0.17 ± 0.09 wt%) in the Linxiang and basal Wufeng formations, followed by an increase to significantly higher concentrations (4.29 ± 1.58 wt%), but with a transient decrease prior to the LOMEI-2 horizon (Fig. 1; see Supplementary Tables 1–4 for all data). Organic C isotope profiles (δ¹³C_{org}) are typical for this time period⁴, with values of ~–29‰ at the base of the succession, followed by an excursion to more negative values and then an increase that starts at the LOMEI-1 horizon and persists until a second decrease coincident with the LOMEI-2 horizon (Fig. 1; Supplementary Fig. 2).

Total phosphorus (P_{tot}) concentrations vary through each section (see Supplementary Note 4 and Supplementary Figs. 4–7 for detailed discussion of P systematics), and this variability is largely controlled by changes in the detrital P pool (Fig. 1). One concern with chemical extractions of P phases is the potential for transfer of authigenic P, particularly carbonate fluorapatite, to more crystalline apatite during diagenesis and metamorphism, which would result in an overestimation of P_{det} at the expense of the P_{aut} pool^{30,31}. However, P_{det} concentrations are also affected by the degree of chemical weathering, whereby more intense chemical weathering would result in enhanced dissolution of apatite and hence lower concentrations of detrital P in sediments delivered to the ocean. Indeed, while P_{det} concentrations are generally low and within the range commonly found in modern continental shelf settings at the more distal site^{27,32}, at the more proximal site, P_{det} increases from the middle of Horizon B to a peak during the glacial interval in Horizon D, followed by a subsequent decrease during the recovery from glaciation (Fig. 1). This apparent paleo-weathering control on P_{det}, which might be expected to be more pronounced in proximal settings, is supported by a strong negative correlation between P_{det} and the chemical index of alteration weathering proxy (Supplementary Fig. 7). Thus, variability in P_{det} (and hence P_{tot}) appears to be largely controlled by climate-induced changes in the intensity of chemical weathering, rather than significant post-depositional transfer of P_{aut} to P_{det}. Possible exceptions to this concern two samples with anomalously high P_{det} (>800 ppm), and four samples from Horizon C in the proximal site, which have elevated P_{det}/Al ratios (shown as open circles on Fig. 1). Some of these samples deviate from the weathering induced trend in P_{det} concentrations (see Supplementary Fig. 7), suggesting potential formation of crystalline apatite during diagenesis, and thus we take a conservative approach whereby these anomalous samples are excluded from further consideration.

Discussion

Based on published redox characteristics for the SH section⁴, combined with new data for the WX drill core (see Supplementary Note 2 for water column redox interpretations), we identify six distinct horizons (Fig. 1). The lower part of Horizon A was deposited under oxic conditions, before anoxic ferruginous (Fe-containing) conditions developed in Horizon B, followed by a transition to weak or intermittent euxinia during the LOMEI-1 interval in Horizon C (Fig. 1). Persistent euxinia then developed

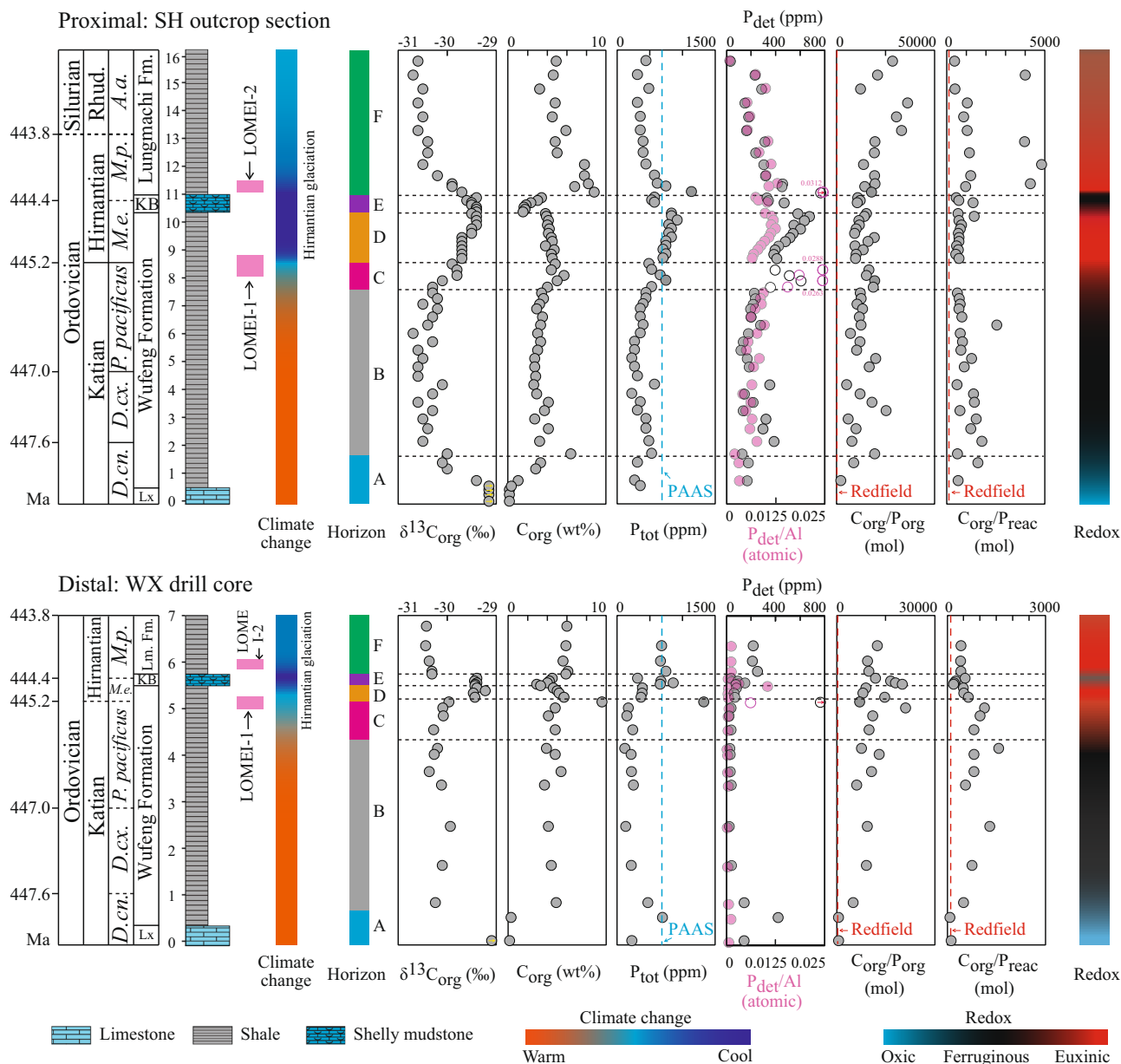


Fig. 1 Geochemical and isotopic data for the proximal Shuanghe (SH) outcrop section and the distal Wuxi (WX) drill core from the Yangtze Shelf Sea, South China. Data for $\delta^{13}C_{org}$, C_{org} , P_{tot} , climate change and redox conditions for the SH section are modified from ref. 4. See Supplementary Information for the climate and redox characterization of the WX drill core. Six stratigraphic horizons (A to F) are distinguished based on these water column redox dynamics. The two extinction intervals of the LOME are denoted as LOMEI-1 and LOMEI-2⁴. Open circles represent samples with anomalous P_{det} contents or P_{det}/Al ratios, which likely represent post-depositional transfer of P_{aut} to P_{det} (see main text and Supplementary Information for details). While this affects C_{org}/P_{react} ratios (and hence the ratios for these samples are discluded from consideration), it does not affect C_{org}/P_{org} ratios. Dashed blue line represents the average P_{tot} concentration for Post-Archean Australian Shale (PAAS). A molar C/P ratio of 106:1 denotes the Redfield ratio (red dashed line). The ages of graptolite zones are from ref. 1. Graptolite zones: *D. cn.* *Dicellograptus complanatus*, *D. cx.* *Dicellograptus complexus*, *P. pacificus* *Paraorthograptus pacificus*, *M. e.* *Metabolograptus extraordinarius*, *M. p.* *Metabolograptus persculptus*, *A. a.* *Akidograptus ascensus*. Rhud. Rhuddanian, Lx Linxiang Formation, KB Kuangyinchiao Bed, Lm.Fm. Lungmachi Formation.

in Horizon D, as well as in Horizon F, the base of which coincides with the LOMEI-2 interval, with Horizon E marking ferruginous (anoxic, Fe-containing) deposition in the interim. Importantly, this ocean redox history is broadly consistent with the reported evolution of ocean redox chemistry at other global sites (Supplementary Fig. 1; Supplementary Table 5).

All samples have molar C_{org}/P_{org} ratios above the Redfield ratio (Figs. 1, 2), consistent with preferential release of P from organic matter during microbial remineralization^{21,33}. Most molar C_{org}/P_{react} ratios (Figs. 1, 2) also fall above the Redfield ratio, and thus

document P_{org} and P_{Fe} recycling back to the water column^{21,26,29}. However, C_{org}/P_{react} ratios are consistently below C_{org}/P_{org} ratios throughout the succession, due to a proportion of the dissolved P being incorporated into authigenic phases. These ratios do, however, show distinct differences between the six horizons (Fig. 2). From Horizon A to C during the Katian stage, C_{org}/P_{org} and C_{org}/P_{react} ratios increase gradually, suggesting a progressive increase in P recycling to the water column (Fig. 3), consistent with the proposed redox evolution from oxic, through ferruginous, to weakly euxinic conditions (Fig. 1). In particular, we note

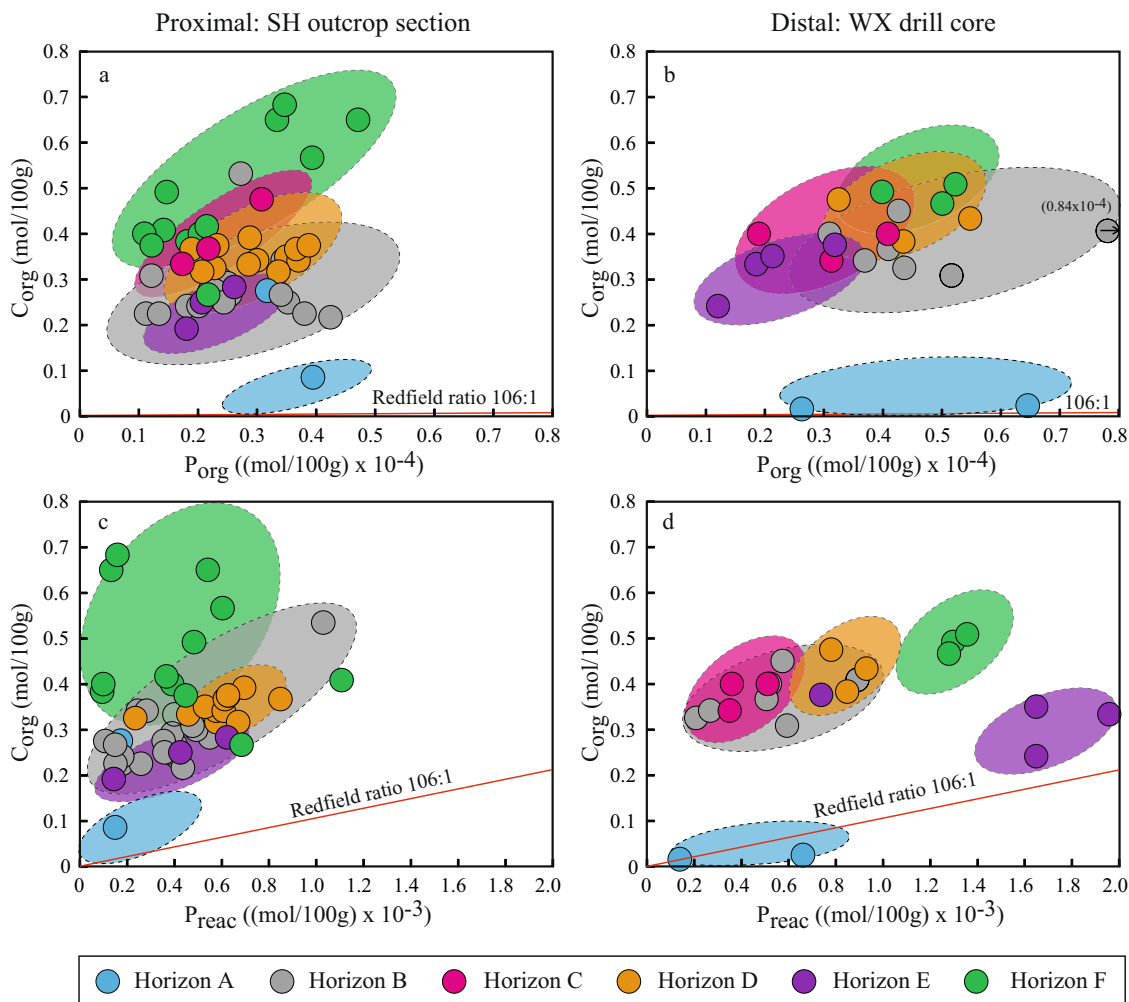


Fig. 2 Molar C_{org}/P_{org} and C_{org}/P_{rec} ratios for the proximal Shuanghe (SH) outcrop section and the distal Wuxi (WX) drill core. **a** C_{org}/P_{org} for the proximal section; **b** C_{org}/P_{org} for the distal section; **c** C_{org}/P_{rec} for the proximal section; **d** C_{org}/P_{rec} for the distal section. Horizons A–F are as identified in Fig. 1, and are broadly grouped into ranges (larger oval groupings). Samples that fall outside of the Horizon A–F groupings on the C_{org}/P_{rec} plots reflect transitional redox conditions at the boundary between different horizons. These samples appear to have been affected by diagenetic over-printing as the redox state of the overlying water column evolved, and thus are not included in the modelling analysis. The red lines represent the molar Redfield ratio of 106:1.

that the sediments deposited under ferruginous conditions document a relatively high degree of pyritization (see Supplementary Table 3 and ref. 4), which suggests that significant sulfide production during diagenesis promoted P recycling, even though the water column itself was not euxinic. These data imply a biogeochemical cascade, whereby enhanced bioavailability of P initially increased marine primary productivity and organic carbon production^{20,34}, thus intensifying oxygen demand in the water column.

The initial increase in bioavailable P may be related to a gradual increase in the weathering influx of P due to early plant evolution¹³, the weathering of volcanic arcs^{35,36}, or deposition of volcanic ash^{17,18}. In this latter regard, the presence of volcanic ash layers supports a pulse of volcanism at the base of the Wufeng Formation (Horizon A), which gradually decreased to Horizon C³⁷, consistent with a mercury (Hg) anomaly taken to indicate enhanced volcanism across this interval³⁸, as well as the presence of mass-independent sulfur isotope anomalies³⁹. The close correspondence between the timing of enhanced volcanism and the initial development of water column anoxia suggests a potential link¹⁸, which may have been particularly pronounced in areas such as the Yangtze shelf Sea, where upwelling likely focused the

supply of bioavailable P⁴⁰, although we note that the initial driver of enhanced P inputs remains unresolved. Nevertheless, while enhanced P bioavailability would have initially promoted oxygen depletion in the water column and sulfide production in the sediments, the consequent enhanced recycling of P from the sediments then tipped the ocean into a weakly euxinic state in Horizon C, which progressed to more intense euxinia in Horizon D (Figs. 1, 3).

During deposition of Horizon D, which marks the onset and progression of the Hirnantian glaciation to its peak (Fig. 1), the intensity of chemical weathering significantly decreased⁴. This would have progressively decreased the weathering influx of sulfate, and sulfate would also have been extensively depleted from the euxinic water column through microbial reduction and removal as pyrite. Global sulfate limitation is supported by an increase in the $\delta^{34}S$ composition of sedimentary pyrite at most sites during deposition of Horizon E (Supplementary Fig. 7; Supplementary Table 5), and this appears to have driven a global change in ocean redox state. However, while ferruginous conditions developed in the Yangtze Shelf Sea area during Horizon E (Figs. 1, 3), other locations appear to have been characterized by the development of oxic to dysoxic conditions. This suggests that

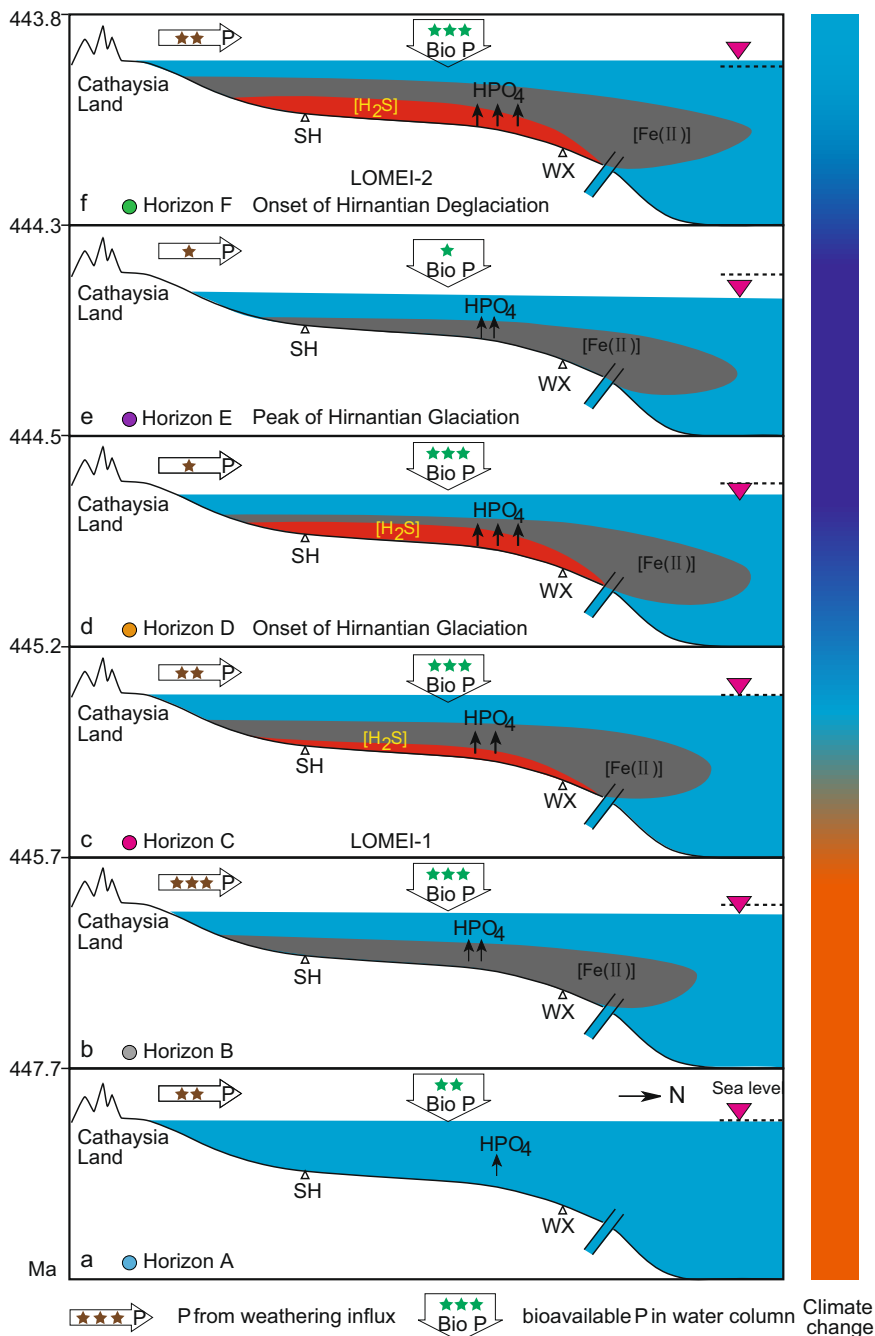


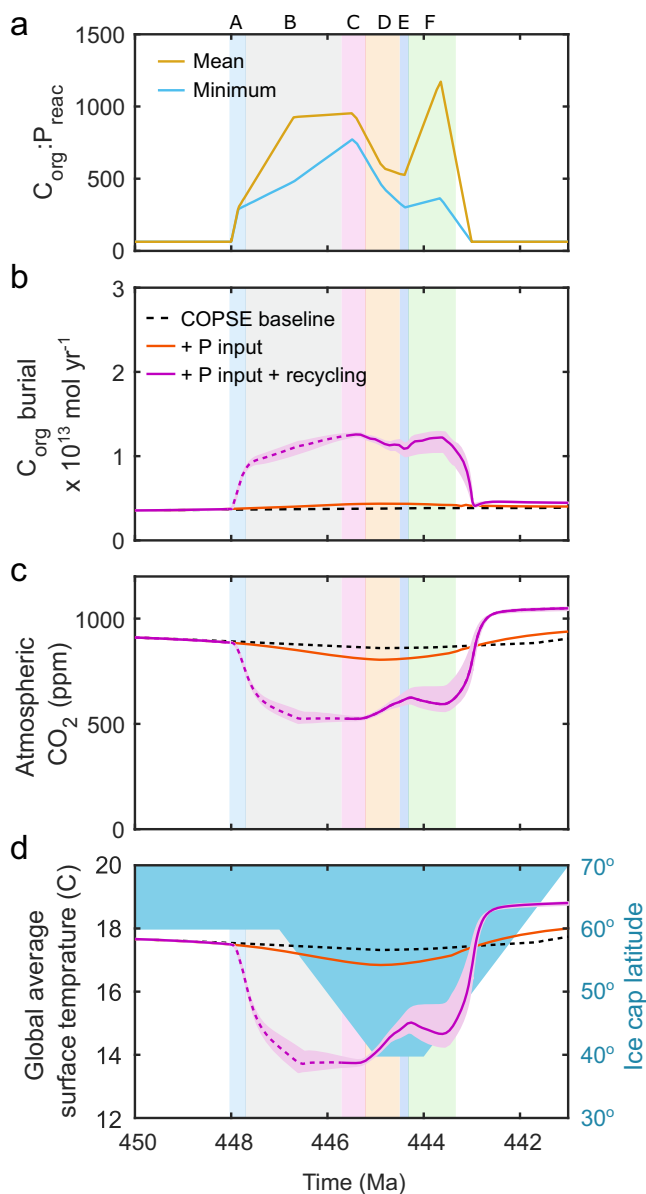
Fig. 3 Conceptual model for the high-resolution redox development and P recycling on Yangtze Shelf Sea in South China. a Horizon A; **b** Horizon B; **c** Horizon C; **d** Horizon D; **e** Horizon E; **f** Horizon F. Two progressive expansions of euxinia led to intense increases in P recycling, which peaked in Horizons C-D and F, and these correspond to the two extinction intervals (LOMEI-1 and LOMEI-2).

the precise nature of the redox transition was controlled by local processes, specifically the depth of the redoxcline, which fluctuated as a function of glacio-eustasy.

Under ferruginous conditions in Horizon E, drawdown of phosphate from the water column in association with Fe minerals would be expected, which is supported by an increase in P_{aut} (likely due to ‘sink switching’ from P_{Fe}), particularly in the more distal setting (Supplementary Fig. 6). Furthermore, the extent of recycling was significantly diminished, as indicated by C_{org}/P_{org} and C_{org}/P_{reac} ratios closer to the Redfield ratio (Fig. 2). This would likely have led to decreased productivity, which is supported by lower organic carbon concentrations (Fig. 1). Less efficient recycling during deposition of Horizon E is also evident

on a global scale, with a general increase in P_{tot} and lower C_{org}/P_{tot} ratios (Supplementary Note 5; Supplementary Fig. 8). This is consistent with the development of oxic or dysoxic conditions at other sites, and supports a global-scale sequestration of the high concentrations of dissolved P produced via recycling during deposition of Horizon D.

Water column sulfate concentrations would be expected to increase progressively after the cessation of euxinic conditions. Indeed, during the onset of deglaciation (Horizon F) there was a return to more widespread water column euxinia both in the Yangtze Shelf Sea (Fig. 3) and globally¹⁰, which may also be related to nutrient and sulfate upwelling during rapid deglaciation^{7,40,41}. Under these conditions, C_{org}/P_{org} and C_{org}/P_{reac}



ratios again increased across the Yangtze Sea transect, suggesting a reintensification of P recycling back to the water column (Fig. 2). This helped to maintain persistent euxinic conditions^{4,10} and high organic carbon production and burial throughout this horizon (Fig. 1).

The Hirnantian glaciation was relatively short-lived, and its apex is thought to have involved ~5 °C of global cooling over a 1–2 Myr timeframe⁷. It is usually assumed that cooling resulted from CO₂ drawdown^{13,35}, and recent proxy estimates of late Ordovician CO₂ point to levels below 1000 ppm⁴². These CO₂ estimations appear consistent with a climate that was similar to the preindustrial (given the reduced solar flux) but substantial uncertainty remains, and previous model-based estimates were much higher⁴³. Recent work has shown that a large volcanic P input event, which occurred coincident with the Hirnantian $\delta^{13}\text{C}$ isotope excursion (HICE)¹⁸, appears to be capable of driving cooling synchronous with the Hirnantian glaciation. This is the only quantitative estimate of Hirnantian P inputs currently available, but biogeochemical modelling suggests that it was not sufficient to drive significant cooling unless there was a high

Fig. 4 COPSE global biogeochemical model with $C_{\text{org}}:P_{\text{reac}}$ imposed based on our geochemical data. a $C_{\text{org}}/P_{\text{reac}}$; b C_{org} burial; c Atmospheric CO₂; d Global average surface temperature and ice cap latitude. Model background run from ref. ⁵⁴ shown as a black dashed line. Red lines show the effects of a pulse of P weathering¹⁸, and purple lines show the combined effect of the same P weathering pulse with additional P recycling, as imposed using the sedimentary $C_{\text{org}}:P_{\text{reac}}$ ratios from our empirical data (shown as the average and lower limit in panel a). The combined model output is shown as a range representing the average and lower limit (where the purple shading represents the average and lower limits, and the purple line represents the mid-point of these two values), in order to provide a conservative estimate for the impact of P recycling. The model predicts substantial increases in P recycling and organic C burial across the interval sampled (b). This also draws down atmospheric CO₂ (c), reducing surface temperature (d). Ice cap latitude is shown in panel d as a blue shaded area, following ref. ³⁶. As discussed in the main text and Supplementary Information, the model results imply a more rapid increase in organic C burial and consequent decrease in CO₂ and temperature across Horizons A and B (shown as a dashed purple line) than suggested by the geologic record. This is attributed to a global overestimation of phosphate bioavailability based on our data from shelf settings, due to subsequent drawdown of recycled phosphate in deeper ocean settings that were poised at a less reducing state than during horizons C–F.

degree of P recycling, estimated at around four times the P input flux¹⁸. Our data show that elevated P recycling during the later Katian and Hirnantian is indeed synchronous with late Ordovician carbon burial brought about by P recycling contributed significantly to the Hirnantian glaciation. If correct, this may explain why the glaciation was relatively short-lived, given that the recycling feedback is a transient phenomenon driven by oceanic redox state. Indeed, a substantial contribution from CO₂ drawdown through enhanced burial of organic carbon, rather than via changes in silicate weathering, is supported by records of increased organic carbon burial^{44,45} during the Hirnantian.

To explore this hypothesis we utilize the COPSE biogeochemical model⁴⁶ (see Methods). We begin with the simulations of ref. ¹⁸, and plot model runs under the assumed enhanced P input from volcanism (i.e., with no recycling) as the red line in Fig. 4. Here, we assume that the maximum estimate of the total P influx from ash deposition and the weathering of tephra was delivered between about 450 and 440 Ma (see Methods). For the next model runs, shown in purple, we alter the COPSE model so that sedimentary P burial is co-constrained by the model rate of organic carbon burial and our measured $C_{\text{org}}:P_{\text{reac}}$ ratio. In this way the model is forced to implement the degree of P recycling observed in the geological record, but is still free to calculate organic carbon burial rates and marine [PO₄] based on its internal biosphere and continental inputs of P. We force the model with the mean $C_{\text{org}}:P_{\text{reac}}$ ratio of our combined proximal and distal datasets, and apply the forcing to 80% of the organic carbon burial flux, which is a conservative estimate for the proportion of organic carbon deposited on the shelf⁴⁷. Here, we note that while there are no other datasets with which to compare our P phase association data, global trends in P_{tot} and $C_{\text{org}}/P_{\text{tot}}$ across horizons A–F provide strong support for the globally representative nature of the relative changes we observe in our $C_{\text{org}}/P_{\text{reac}}$ data (Supplementary Fig. 8; Supplementary Table 5).

Our full model results (Fig. 4) show that changes to the P recycling rate derived from our data result in substantial changes to the carbon cycle. As sedimentary $C_{\text{org}}/P_{\text{reac}}$ ratios begin to increase across Horizons A–C, the global rate of organic carbon burial more than doubles, and atmospheric CO₂ concentration is

reduced from around 900 ppm to around 500 ppm. This causes ~4 °C of global cooling between the earlier Katian and the main phase of Hirnantian glaciation, which is similar to the decrease predicted by isotopic temperature proxies^{7,48} (although oxygen isotope temperature proxies tend to predict higher temperatures overall⁴⁹). The model also produces a simplified carbonate-carbon isotope ($\delta^{13}\text{C}_{\text{carb}}$) record, and this records a positive excursion of around 7‰, similar to the observed Hirnantian $\delta^{13}\text{C}_{\text{carb}}$ excursion (Supplementary Fig. 9). As expected, organic C burial is reduced during Horizon E where euxinia abates and P recycling is curtailed, and then increases again during Horizon F when shelf euxinia returns (Fig. 4). In fact, on a global scale, the decrease in organic C burial during Horizon E was likely even greater, since our identification of a degree of P recycling under ferruginous conditions on the Yangtze Shelf (Fig. 2) appears to contrast with more extensive P drawdown under oxic-dysoxic conditions in other global localities (Supplementary Fig. 8; Supplementary Table 5).

The model temperature prediction is compared qualitatively to the expansion of ice caps from the geological record³⁶ (Fig. 4d). The timing of ice cap advance and retreat, which occurs between ~447 and ~442 Ma shows a reasonable agreement with our model predictions, although the model has the onset of cooling earlier, between 448 and 447 Ma (Fig. 4d), and also predicts an earlier onset of the positive $\delta^{13}\text{C}_{\text{carb}}$ excursion than is observed in the $\delta^{13}\text{C}_{\text{carb}}$ record (Supplementary Note 6; Supplementary Fig. 9). This may be explained by the simplicity of the model and its input variables, which are not defined at sufficiently high resolution and lack spatial characteristics that are important for calculating continental surface processes. In particular, the moderate level of P recycling recorded under ferruginous conditions in Horizon B drives the beginning of the carbon burial event (Figs. 2, 4). However, during these early stages of anoxia, it is likely that the global deeper ocean would have been poised at an overall less reducing state, which would have promoted drawdown of recycled phosphate^{25,32}, thus reducing the global bioavailability of P. This deeper ocean drawdown of P during the initiation of shallower water anoxia is not factored into our biogeochemical model, which thus results in an earlier onset of CO₂ drawdown. Nevertheless, despite this discrepancy, the fact that our model reproduces both the observed ~7‰ $\delta^{13}\text{C}_{\text{carb}}$ excursion and a multi-million-year negative temperature shift by several degrees, supports the suggestion that P recycling played a critical role in driving the Hirnantian glaciation.

Conclusions

Our high-resolution reconstruction of redox and P recycling on the Yangtze Shelf Sea in South China clearly demonstrates two expansions of euxinia and associated rises in P recycling during the late Ordovician (Fig. 3). Once anoxia was established, the increased recycling of P promoted a major increase in marine primary productivity. This not only drove the two extinction phases of the LOME through the development of euxinic conditions, but also resulted in large-scale CO₂ drawdown and transient deep glaciation during the Hirnantian, which played a secondary role in driving the extinction of certain low-latitude taxa⁴. We thus conclude that redox-promoted P recycling was a critical factor in driving Earth's first major extinction of animal life.

Methods

Total organic carbon (C_{org}) and carbon isotope ($\delta^{13}\text{C}_{\text{org}}$) analyses. Samples for all analyses were collected by the authors and no permissions were required. C_{org} and $\delta^{13}\text{C}_{\text{org}}$ values for the proximal Shuanghe inner-shelf (SH) outcrop section are from ref. 4. For samples from the distal outer-shelf Wuxi (WX) drill core section, sample powders were decarbonated with HCl (10% vol/vol) prior to C_{org} analysis

on a LECO CS-230 analyzer. Analytical precision for C_{org} was generally better than 5%. Sample powders for $\delta^{13}\text{C}_{\text{org}}$ measurements were also first decarbonated with HCl (10% vol/vol). The decalcified samples were combusted for isotopic analysis using cryogenically purified CO₂ in a Finnigan MAT-253 mass spectrometer. All $\delta^{13}\text{C}_{\text{org}}$ data are reported in standard δ -notation relative to the Vienna Pee Dee Belemnite (VPDB) standard, with a precision of $\pm 0.1\%$ (1 σ level).

Elemental concentrations. Major (Fe_T and P_{tot}) and trace elements (Mo and U) in the distal outer-shelf Wuxi (WX) drill core section were measured by the methods in ref. 4. Sample powders for major elements were heated and mixed with flux (Li₂B₄O₇) in a proportion of 1:5 before analysis. Sample powders for trace elements were dissolved with HF + HNO₃ prior to analysis. Major elements were measured by X-ray fluorescence spectrometry (XRF-1500), and trace elements were measured on a VG PQ2 Turbo inductively coupled plasma source mass spectrometer (FINNIGAN MAT). Analytical precision was better than 3% for all elements of interest.

Fe-S systematics. For the operationally defined Fe extraction method⁵⁰, Fe_{carb} (targeting Fe in carbonate minerals, including siderite and ankerite) was extracted with a sodium acetate solution (pH = 4.5) for 48 h at 50 °C, Fe_{ox} (targeting Fe (oxyhydr)oxide minerals) was extracted with a citrate-dithionite-acetate solution (pH = 4.8) for 2 h at room temperature, and Fe_{mag} (targeting mixed ferrous-ferric phases, particularly magnetite) was extracted with an ammonium oxalate solution for 6 h at room temperature. These three steps were performed sequentially, with the extracted Fe measured by atomic adsorption spectroscopy. Fe_{AVS} (acid volatile sulfide) and Fe_{py} (pyrite) were extracted by the two step-acid Cr(II) method⁵¹, with concentrations determined gravimetrically. Replicate analysis gave RSDs of <5% for all phases, and accuracy was confirmed relative to an Fe speciation reference material (WHIT)⁵².

P phase partitioning. A recently revised sequential extraction method³⁰ was used to determine the phase partitioning of P. P_{Fe1} (which targets poorly crystalline Fe (oxyhydr)oxide-bound P) was extracted with a dithionite-citrate-bicarbonate solution (pH 7.6) for 8 h at room temperature. Authigenic P (P_{auth}; which targets carbonate fluorapatite) was extracted with a sodium acetate solution at pH 4 for 6 h at room temperature. Detrital apatite (P_{det}) was extracted with a 10% HCl solution for 16 h at room temperature. P_{mag} (which targets P associated with magnetite) was extracted with an ammonium oxalate solution for 6 h at room temperature. P_{Fe2} (which targets more crystalline Fe (oxyhydr)oxide minerals) was extracted with a dithionite-citrate-acetate solution (pH 4.8) for 8 h at room temperature. Finally, the residue was ashed (550 °C for 2 h) and reacted with 10% HCl for 16 h at room temperature to liberate organic-bound P (P_{org}). The sum of P_{Fe1} + P_{Fe2} + P_{mag} gives P_{Fe}. The P content of the various extracts was determined either spectrophotometrically via the molybdate blue method⁵³, or by ICP-OES for solutions where the matrix interferes with the molybdate blue method (P_{Fe1}, P_{Fe2} and P_{mag}). Replicate extractions gave RSDs of <2.1% for P_{Fe1}, <2.2% for P_{auth}, <2.9% for P_{det}, <1.0% for P_{mag}, <1.0% for P_{Fe2}, and <2.0% for P_{org}.

Biogeochemical modeling. We use the COPSE (Carbon Oxygen Phosphorus Sulfur Evolution) global biogeochemical model⁵⁴. COPSE is an extension of the GEOCARB⁵⁵ box model framework, which incorporates a dynamic biosphere. We use the latest model version⁵⁴, which provides a 'baseline' run through the Paleozoic Era. A key uncertainty in this previous run is the degree to which the evolution of vascular land plants enhanced continental weathering rates⁵⁶, which alters background conditions in the prevascular world, and which we set here at a factor of 0.5 relative to present day, resulting in background Ordovician CO₂ concentrations of around 1000 ppm, close to proxy estimates⁴². To produce the red lines in Fig. 4 we use the model baseline and add an assumed enhancement of P weathering inputs in line with previously published work¹⁸. This is a gaussian increase in P input between 450 and 440 Ma, with a total flux of 4.59×10^{16} mol P, taken directly from the maximum estimates of ref. 18, assuming weathering continued for the entire 10 Myr input timeframe. We also alter the P burial functions to calculate total marine P burial based on the model organic C burial rate and the $\text{C}_{\text{org}}:\text{P}_{\text{reac}}$ ratio from our dataset (purple lines). When $\text{C}_{\text{org}}:\text{P}_{\text{reac}}$ rises substantially above the Redfield ratio, the P burial term becomes very small, and most potentially bioavailable P is recycled from the sediment. The model P burial is calculated as (1):

$$P_{\text{burial}} = \frac{f_{\text{shelf}} F_{\text{moch}}}{CP_{\text{reac}}} + \frac{(1 - f_{\text{shelf}}) F_{\text{moch}}}{CP_{\text{reac0}}} \quad (1)$$

where f_{shelf} is the fraction of organic carbon burial that occurs on the shelf, taken as 0.8. F_{moch} is the marine organic carbon burial rate, CP_{reac} is the measured $\text{C}_{\text{org}}:\text{P}_{\text{reac}}$ ratio, and CP_{reac0} is the first value in our dataset to which the model is initiated. This formulation therefore assumes that the deep ocean P burial flux is unaffected by the dynamics we observe in our sections. Note also that we do not assume that organic carbon burial is directly affected by anoxia. Increasing F_{moch} in this way would bury more P for a given CP_{reac} , which would reduce the P recycling flux. However, this would be countered by having buried more organic carbon in the first place, and would still produce a C_{org} burial event.

Data availability

All data generated during this study are included in the Supplementary Information and are available at EarthChem (<https://doi.org/10.26022/IEDA/112232>).

Code availability

The COPSE model can be downloaded for free at bjwmills.com.

Received: 26 August 2021; Accepted: 10 March 2022;

Published online: 05 April 2022

References

- Fan, J. et al. A high-resolution summary of Cambrian to Early Triassic marine invertebrate biodiversity. *Science* **367**, 272–277 (2020).
- Harper, D. A. T., Hammarlund, E. U. & Rasmussen, C. M. Ø. End Ordovician extinctions: a coincidence of causes. *Gondwana Res.* **25**, 1294–1307 (2014).
- Hammarlund, E. U. et al. A sulfidic driver for the end-Ordovician mass extinction. *Earth Planet. Sci. Lett.* **331–332**, 128–139 (2012).
- Zou, C. et al. Ocean euxinia and climate change ‘double whammy’ drove the Late Ordovician mass extinction. *Geology* **46**, 535–538 (2018).
- Bartlett, R. et al. Abrupt global-ocean anoxia during the Late Ordovician–Early Silurian detected using uranium isotopes of marine carbonates. *Proc. Natl Acad. Sci. USA* **115**, 5896–5901 (2018).
- Vandenbroucke, T. R. A. et al. Polar front shift and atmospheric CO₂ during the glacial maximum of the Early Paleozoic Icehouse. *Proc. Natl Acad. Sci. USA* **107**, 14983–14986 (2010).
- Finnegan, S. et al. The magnitude and duration of Late Ordovician–Early Silurian glaciation. *Science* **331**, 903–906 (2011).
- Saupe, E. E. et al. Extinction intensity during Ordovician and Cenozoic glaciations explained by cooling and palaeogeography. *Nat. Geosci.* **13**, 65–70 (2020).
- Ahm, A. S. C., Bjerrum, C. J. & Hammarlund, E. U. Disentangling the record of diagenesis, local redox conditions, and global seawater chemistry during the latest Ordovician glaciation. *Earth Planet. Sci. Lett.* **459**, 145–156 (2017).
- Stockey, R. G. et al. Persistent global marine euxinia in the early Silurian. *Nat. Commun.* **11**, 1804 (2020).
- Kump, L. R. et al. A weathering hypothesis for glaciation at high atmospheric pCO₂ during the Late Ordovician. *Palaeogeogr. Palaeoclimatol. Palaeoecol.* **152**, 173–187 (1999).
- Finlay, A. J., Selby, D. & Grocke, D. R. Tracking the Hirnantian glaciation using Os isotopes. *Earth Planet. Sci. Lett.* **293**, 339–348 (2010).
- Lenton, T., Crouch, M., Johnson, M., Pires, N. & Dolan, L. First plants cooled the Ordovician. *Nat. Geosci.* **5**, 86–89 (2012).
- Lenton, C. M. O. et al. Earliest land plants created modern levels of atmospheric oxygen. *Proc. Natl Acad. Sci. USA* **113**, 9704–9709 (2016).
- Kenrick, P., Wellman, C., Schneider, H. & Edgecombe, G. A timeline for terrestrialization: consequences for the carbon cycle in the Palaeozoic. *Phil. Trans. R Soc. Lond. B* **367**, 519–536 (2012).
- Porada, P. et al. High potential for weathering and climate effects of nonvascular vegetation in the Late Ordovician. *Nat. Commun.* **7**, 12113 (2016).
- Buggisch, W. et al. Did intense volcanism trigger the first Late Ordovician icehouse? *Geology* **38**, 327–330 (2010).
- Longman, J. et al. Volcanic nutrient supply initiated Late Ordovician climate change and extinctions. *Nat. Geosci.* **14**, 924–929 (2021).
- Tyrrell, T. The relative influences of nitrogen and phosphorus on oceanic primary production. *Nature* **400**, 525–531 (1999).
- Van Cappellen, P. & Ingall, E. D. Redox stabilization of the atmosphere and oceans by phosphorus-limited marine productivity. *Science* **271**, 493–496 (1996).
- Ingall, E. D., Bustin, R. M. & Cappellen, P. V. Influence of water column anoxia on the burial of organic carbon and phosphorus in marine shales. *Geochim. Cosmochim. Acta* **57**, 303–316 (1993).
- Ingall, E. D. & Jahnke, R. Evidence for enhanced phosphorus regeneration from marine sediments overlain by oxygen depleted waters. *Geochim. Cosmochim. Acta* **58**, 2571–2575 (1994).
- Algeo, T. J. et al. Changes in productivity and redox conditions in the Panthalassic Ocean during the latest Permian. *Geology* **38**, 187–190 (2010).
- Bowyer, F. T. et al. Regional nutrient decrease drove redox stabilisation and metazoan diversification in the late Ediacaran Nama Group, Namibia. *Sci. Rep.* **10**, 2240 (2020).
- Schobben, M. et al. A nutrient control on marine anoxia during the end-Permian mass extinction. *Nat. Geosci.* **13**, 640–646 (2020).
- Dale, A. W., Boyle, R. A., Lenton, T. M., Ingall, E. D. & Wallmann, K. A model for microbial phosphorus cycling in bioturbated marine sediments: Significance for phosphorus burial in the early Paleozoic. *Geochim. Cosmochim. Acta* **189**, 251–268 (2016).
- Ruttenberg, K. C. Development of a sequential extraction method for different forms of phosphorus in marine sediments. *Limnol. Oceanogr.* **37**, 1460–1482 (1992).
- Egger, M., Jilbert, T., Behrends, T., Rivard, C. & Slomp, C. P. Vivianite is a major sink for phosphorus in methanogenic coastal surface sediments. *Geochim. Cosmochim. Acta* **169**, 217–235 (2015).
- Xiong, Y. et al. Phosphorus cycling in Lake Cadagno, Switzerland: a low sulfate euxinic ocean analogue. *Geochim. Cosmochim. Acta* **251**, 116–135 (2019).
- Thompson, J. et al. Development of a modified SEDEX phosphorus speciation method for ancient rocks and modern iron-rich sediments. *Chem. Geol.* **524**, 383–393 (2019).
- Creveling, J. R. et al. Phosphorus sources for phosphatic Cambrian carbonates. *Geol. Soc. Am. Bull.* **126**, 145–163 (2014).
- Guilbaud, R. et al. Phosphorus-limited conditions in the early Neoproterozoic ocean maintained low levels of atmospheric oxygen. *Nat. Geosci.* **13**, 296–301 (2020).
- Krom, M. D. & Berner, R. A. The diagenesis of phosphorus in a nearshore marine sediment. *Geochim. Cosmochim. Acta* **45**, 207–216 (1981).
- Bjerrum, C. J., Bendtsen, J. & Legarth, J. J. F. Modeling organic carbon burial during sea level rise with reference to the Cretaceous. *Geochem. Geophys. Geosyst.* **7**, Q05008 (2006).
- Young, S. A. et al. A major drop in seawater ⁸⁷Sr/⁸⁶Sr during the Middle Ordovician (Darriwilian): Links to volcanism and climate? *Geology* **37**, 951–954 (2009).
- Macdonald, F. A. et al. Arc-continent collisions in the tropics set Earth’s climate state. *Science* **364**, 181–184 (2019).
- Qiu, Z. & Zou, C. Unconventional petroleum sedimentology: connotation and prospect. *Acta Sediment. Sin.* **38**, 1–29 (2020).
- Hu, D. et al. Major volcanic eruptions linked to the Late Ordovician mass extinction: Evidence from mercury enrichment and Hg isotopes. *Glob. Planet. Chang.* **196**, 103374 (2021).
- Hu, D. et al. Large mass independent sulphur isotope anomalies link stratospheric volcanism to the Late Ordovician mass extinction. *Nat. Commun.* **11**, 2297 (2020).
- Yang, S., Hu, W. & Wang, X. Mechanism and implications of upwelling from the Late Ordovician to early Silurian in the Yangtze region, South China. *Chem. Geol.* **565**, 120074 (2021).
- Rong, J. Y. et al. The latest Ordovician Hirnantian brachiopod faunas: new global insights. *Earth Sci. Rev.* **208**, 103280 (2020).
- Witkowski, C. R. et al. Molecular fossils from phytoplankton reveal secular PCO₂ trend over the Phanerozoic. *Sci. Adv.* **4**, eaat4556 (2018).
- Berner, R. A. & Kothavala, Z. Geocarb III: a revised model of atmospheric CO₂ over Phanerozoic time. *Am. J. Sci.* **301**, 182–204 (2001).
- Brenchley, P. et al. High-resolution stable isotope stratigraphy of Upper Ordovician sequences: constraints on the timing of bioevents and environmental changes associated with mass extinction and glaciation. *Geol. Soc. Am. Bull.* **115**, 89–104 (2003).
- Shen, J. et al. Improved efficiency of the biological pump as a trigger for the Late Ordovician glaciation. *Nat. Geosci.* **11**, 510–514 (2018).
- Lenton, T. M. et al. COPSE reloaded: an improved model of biogeochemical cycling over Phanerozoic time. *Earth Sci. Rev.* **178**, 1–28 (2018).
- Slomp, C. P. & Van Cappellen, P. The global marine phosphorus cycle: sensitivity to oceanic circulation. *Biogeosciences* **4**, 155–171 (2007).
- Scotese, C. R. et al. Phanerozoic Paleotemperatures: The Earth’s Changing Climate during the Last 540 million years. *Earth Sci. Rev.* **215**, 103503 (2021).
- Grossman, E. L. & Joachimski, M. M. in *Geologic Time Scale 2020*, 279–307, (Elsevier, 2020).
- Poulton, S. W. & Canfield, D. E. Development of a sequential extraction procedure for iron: implications for iron partitioning in continentally derived particulates. *Chem. Geol.* **214**, 209–221 (2005).
- Canfield, D. E. et al. The use of chromium reduction in the analysis of reduced inorganic sulfur in sediments and shales. *Chem. Geol.* **54**, 149–155 (1986).
- Alcott, L. et al. Development of iron speciation reference materials for palaeoredox analysis. *Geostand. Geoanal. Res.* **44**, 581–591 (2020).
- Strickland, J. D. H. & Parsons, T. R. in *A Practical Handbook of Seawater Analysis*, 2nd edn., 167, 45–64 (Fisheries Research Board of Canada, Ottawa, Bulletin, 1972).
- Tostevin, R. & Mills, B. J. W. Reconciling proxy records and models of Earth’s oxygenation during the Neoproterozoic and Palaeozoic. *Interface Focus* **10**, 20190137 (2020).
- Berner, R. A. A model for atmospheric CO₂ over Phanerozoic time. *Am. J. Sci.* **291**, 339–376 (1991).
- Lenton, T. The role of land plants, phosphorus weathering and fire in the rise and regulation of atmospheric oxygen. *Global Chang. Biol.* **7**, 613–6297 (2001).

Acknowledgements

This work was supported by NSFC (grants 41888101 and 41602119) and the Scientific Research and Technological Development Program of CNPC (2021yjca02). B.J.W.M. and

S.W.P. are supported by the UK Natural Environment Research Council (grants NE/S009663/1 and NE/R010129/1), and S.W.P. acknowledges support from a Royal Society Wolfson Research Merit Award. We thank Christian Bjerrum for useful comments on earlier versions of the manuscript, Tianchen He for helpful discussion, and Hongyan Wang, Qun Zhao, and Dazhong Dong for assistance with sampling and geochemical analysis. We are also grateful to professors Rixing Zhu, Jiayu Rong, Xu Chen, Pingan Peng, Chengshan Wang, Shuzhong Shen, Zhijun Jin, and Fang Hao of the Chinese Academy of Sciences for helpful discussions.

Author contributions

C.N.Z., Z.Q., and S.W.P. designed the research. Z.Q., H.F.T., and B.L. collected samples. Z.Q., Y.J.X., H.F.T., and H.L.L. performed analyses. Z.Q., S.W.P., B.J.W.M., C.N.Z., and W.J.X. interpreted the data. Z.Q., S.W.P., and B.J.W.M. wrote the manuscript, with contributions from all co-authors.

Competing interests

The authors declare no competing interests.

Additional information

Supplementary information The online version contains supplementary material available at <https://doi.org/10.1038/s43247-022-00412-x>.

Correspondence and requests for materials should be addressed to Zhen Qiu, Caineng Zou or Simon W. Poulton.

Peer review information *Communications Earth & Environment* thanks Kazumi Ozaki, Ellery Ingall and the other, anonymous, reviewer(s) for their contribution to the peer review of this work. Primary Handling Editors: Joe Aslin, Heike Langenberg.

Reprints and permission information is available at <http://www.nature.com/reprints>

Publisher's note Springer Nature remains neutral with regard to jurisdictional claims in published maps and institutional affiliations.



Open Access This article is licensed under a Creative Commons Attribution 4.0 International License, which permits use, sharing, adaptation, distribution and reproduction in any medium or format, as long as you give appropriate credit to the original author(s) and the source, provide a link to the Creative Commons license, and indicate if changes were made. The images or other third party material in this article are included in the article's Creative Commons license, unless indicated otherwise in a credit line to the material. If material is not included in the article's Creative Commons license and your intended use is not permitted by statutory regulation or exceeds the permitted use, you will need to obtain permission directly from the copyright holder. To view a copy of this license, visit <http://creativecommons.org/licenses/by/4.0/>.

© The Author(s) 2022